# First-principles study of strain-electronic interplay in ZnO: Stress and temperature dependence of the piezoelectric constants

Nicola A. Hill
*Materials Department, University of California, Santa Barbara, California 93106-5050*

Umesh Waghmare*
*Department of Physics, Harvard University, Cambridge, Massachusetts 02138*

(Received 21 April 2000)

We present a first-principles study of the relationship between stress, temperature, and electronic properties in piezoelectric ZnO. Our method is a plane wave pseudopotential implementation of density-functional theory and density-functional linear response within the local-density approximation. We observe marked changes in the piezoelectric and dielectric constants when the material is distorted. This stress dependence is the result of strong, bond-length dependent hybridization between the O $2p$ and Zn $3d$ electrons. Our results indicate that fine tuning of the piezoelectric properties for specific device applications can be achieved by control of the ZnO lattice constant, for example by epitaxial growth on an appropriate substrate.

## I. INTRODUCTION

Zinc oxide (ZnO) is a tetrahedrally coordinated wide band gap semiconductor that crystallizes in the wurtzite structure (Fig. 1). The lack of center of symmetry, combined with a large electromechanical coupling, result in strong piezoelectric properties, and the consequent use of ZnO in mechanical actuators and piezoelectric sensors. In addition, ZnO is transparent to visible light and can be made highly conductive by doping. This leads to applications in surface acoustic wave devices and transparent conducting electrodes. However the piezoelectric properties can change the characteristics of potential energy barriers to mobile charges at interfaces, and hence affect the carrier transport properties. The resulting piezoresistance is at times desirable, for example, in ZnO-based metal-oxide varistors which can dissipate large amounts of power in short response times and are commonly found as electrical surge protectors.[1] However, the detailed effects of piezoelectrically induced changes on the electrical behavior of ZnO have not yet been well characterized, and as ZnO finds increased application in electronic devices these effects will have large technological impact.

In this paper we present a first-principles study of the strain dependence of the electrical properties of ZnO, using a plane-wave pseudopotential implementation of density-functional theory (DFT) within the local-density approximation (LDA). We calculate and analyze the structural dependence of total energies, band structures and piezoelectric and dielectric constants. The principal result of our analysis is that the piezoelectric constants of ZnO are strongly dependent on conditions of stress and temperature, whereas the dielectric coefficients vary less strongly. Of particular interest is a comparison of the properties of ZnO, in which the Zn $3d$ bands are filled, with those of $PbTiO_3$, which has empty Ti $3d$ states. Both materials have anomalously large piezoelectric coefficients, but in $PbTiO_3$ the dielectric coefficients are also anomalously large, whereas ZnO behaves as an ordinary dielectric. Our hypothesis is that the strong O $2p$–Zn $3d$ hybridization, which has been previously noted in $PbTiO_3$,[2,3] also occurs in ZnO, leading in both materials to strong strain-phonon coupling and consequently large piezoelectric coefficients. Thus a filled $3d$ band does not preclude a large piezoelectric response. The large dielectric response in $PbTiO_3$ has a similar origin. In ZnO however, the filled O $2p$ and Zn $3d$ bands do not allow a large orbital response to an applied electric field, resulting in a normal dielectric response.

The remainder of this paper is organized as follows. In Sec. II we summarize the results of earlier theoretical studies of ZnO. In Sec. III we describe the theoretical and computational methods used in this work. In Sec. IV, we describe our results for the static and response properties of bulk ZnO at its equilibrium lattice constant. In Sec. V we investigate the dependence of the electronic structure and response functions on external stress or changes in temperature. Finally, in Sec. VI we present our conclusions and discuss implications for materials growth and device design.

## II. PREVIOUS THEORETICAL WORK

First-principles studies of ZnO are computationally challenging. First, the wurtzite structure contains twice as many atoms per unit cell as the zincblende semiconductor structure. In addition, both oxygen and zinc are problematic atoms for the construction of pseudopotentials. In both cases the relevant valence electrons (O $2p$ and Zn $3d$) have no

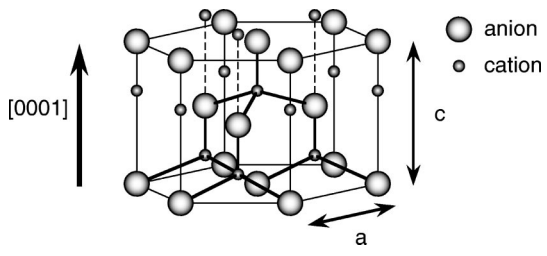


FIG. 1. The wurtzite structure of ZnO.

 

lower-lying electrons of the same angular momentum to provide an effective repulsive potential from the orthogonalization requirement.[4] As a result they are tightly bound and require a large number of plane waves in their expansion.

A band structure of ZnO (Ref. 5) was calculated over 30 years ago using the Green's-function Korringa-Kohn-Rostoker method. This was followed by empirical pseudopotential calculations[6,7] in which the Zn $3d$ electrons were placed in the core. In addition to preventing assessment of the Zn $3d$ contribution to bonding properties, this approach was later shown to give unsatisfactory results.[8]

Schroer and co-workers[8] circumvented the problem of a large plane-wave basis set by combining the use of pseudopotentials with localized Gaussian basis sets containing orbitals of $s$, $p$, $d$, and $s^*$ symmetry. Using this basis they compared the results of LDA calculations using $Zn^{2+}$ (in which the $3d$ electrons are contained in the core) and $Zn^{12+}$ (in which the $3d$ electrons are valence electrons) pseudopotentials, and found that the $Zn^{12+}$ pseudopotential gave results in good agreement with experiment. For example, their LDA energy minimum volume was 0.6% below the experimental value and their calculated band structure was in reasonable agreement with angle-resolved photoemission measurements. There was a slight discrepancy in the position of the $d$ bands which they attributed to inadequacy of the local density approximation in describing these strongly correlated bands.

Dal Corso *et al.*[9] avoided the use of pseudopotentials entirely by using the all electron full potential linear augmented plane-wave (FLAPW) method. They calculated the piezoelectric and polarization properties of ZnO within the LDA, with the purpose of determining the origin of the unusually strong piezoelectric response in ZnO. The principal result of their work was that the contribution to the macroscopic polarization tensor from the relative displacement of the sublattices was large, and only partly canceled by the electronic ''clamped-ion'' contribution, leading to a large net piezoelectric polarization. (In contrast, in zincblende semiconductors these terms are of similar magnitude and opposite sign, resulting in a small piezoelectric polarization.) As in Ref. 8, their LDA volume slightly underestimated the experimental value, and their Zn $d$ bands were around 4 eV higher in energy than observed in photoemission.

Hartree-Fock calculations have been used successfully to determine the stability of, and transitions between, different phases of ZnO (Ref. 10) and to calculate the $(10\bar{1}0)$ surface reconstruction for the wurtzite phase.[11] The Hartree-Fock approximation also gives an incorrect energy position for the Zn $3d$ bands—this time around 2 eV too low.

## III. COMPUTATIONAL TECHNIQUES

### A. Pseudopotential construction

The calculations described in this work were performed using a plane-wave pseudopotential implementation[12] of density-functional theory[13] within the local-density approximation. Plane-wave basis sets offer many advantages in total-energy calculations for solids, including completeness, an unbiased representation, and arbitrarily good convergence accuracy. They also allow for straightforward mathematical formulation and implementation, which is invaluable in the calculation of Hellmann-Feynman forces[14] and in the density-functional theory linear-response calculations employed here.[15]

However, plane-wave basis sets necessitate the use of pseudopotentials to model the electron-ion interaction, in order to avoid rapid oscillations of the valence wave functions in the region around the ion cores. The difficulties associated with applying the pseudopotential method to tightly bound $d$ electrons, which might be expected to require a prohibitively large number of plane waves to expand their pseudopotentials, were mentioned above. An earlier study of cubic ZnS (Ref. 16) using the smooth Trouiller-Martins pseudopotentials, required plane waves up to 121 Ry in energy to achieve an energy convergence of 0.05 eV. Although feasible for a bulk calculation for the zincblende structure (with only two atoms per unit cell) such a large energy cutoff is undesirable for larger unit cells, such as that of the wurtzite structure, or those required for calculation of surface properties. In this work, we use the optimized pseudopotentials developed by Rappe *et al.*,[17] which allow us to reduce the required energy cutoff to 64 Ry without compromising accuracy or transferability. Optimized pseudopotentials minimize the kinetic energy in the high Fourier components of the pseudowavefunction, leading to a corresponding reduction in the contribution of high Fourier components in the solid.

For both Zn and O we constructed nonrelativistic optimized pseudopotentials. The oxygen pseudopotentials were generated from a $2s^2 2p^4$ reference configuration with core radii, $r_c$, of 1.5 a.u. for both $s$ and $p$ orbitals. They were then optimized using 4 and 3 basis functions with cutoff wave vectors, $q_c$, of 7.0 and 6.5 a.u. for $s$ and $p$ orbitals, respectively. $q_c$ determines the convergence of the kinetic energy with respect to the plane-wave cutoff energy in reciprocal-space calculations. These oxygen pseudopotentials were used in earlier calculations for perovskite oxides,[18,19] and gave accurate results. The zinc pseudopotentials were constructed for a neutral Zn atom with reference configuration $3d^{10}4s^{1.75}4p^{0.25}$. $r_c$ values of 2.0, 1.4, and 1.4 a.u.s were used for $d$, $s$, and $p$ orbitals, respectively, with $q_c$ values of 8.0, 7.0, and 8.0 Ry (giving a cutoff energy of 64 Ry.) The transferability of the pseudopotential was tested for a variety of $+1$ and $+2$ free Zn ions. The pseudototal energies and eigenvalues were in agreement with all the electron values to within 0.001 a.u.s. There was no improvement in transferability, or in agreement with all electron calculations for bulk systems, on inclusion of nonlinear core corrections.[20] All pseudopotentials were put into separable form[21] using one projector for each angular momentum. For both Zn and O the $l=1$ component was chosen as the local potential. The absence of ghost states was confirmed using the ghost theorem of Gonze, Käckell, and Scheffler.[22]

### B. Density-functional theory linear response

We use density-functional theory linear-response (DFT-LR) to obtain the quadratic couplings between homogeneous strain, internal displacements of atoms and macroscopic electric field.[23] We use a variational formulation of DFT-LR (Ref. 24) in which the second derivative of total energy is minimized with respect to the first derivatives of Kohn-Sham wave functions with appropriate orthogonality constraints.

This method avoids using any finite-difference formulas and yields dielectric or piezoelectric constants with a minimal number of calculations.

To obtain the piezoelectric and dielectric constants, we calculate the DFT-LR of our system to two types of perturbations: (a) phonon (or atomic displacements) and (b) electric field. Using the first-order response wave function resulting from (a) in the Hellman-Feynman force formula[14] and in the stress formula,[25] we obtain the dynamical matrix and the coupling between phonons and strain, respectively. Similarly, the response wave functions resulting from (b) are used to obtain the Born effective charges and the clamped-ion piezoelectric constants respectively.

The symmetry of the wurtzite structure allows three independent piezoelectric constants ($\gamma_{33}, \gamma_{13}, \gamma_{14}$) and two dielectric constants ($\epsilon_{33}, \epsilon_{13}$). In the present work, we focus on $\gamma_{33}$, $\gamma_{13}$, and $\epsilon_{33}$. The piezoelectric constants $\gamma_{33}$ and $\gamma_{13}$ give the polarization along the *c*-axis induced by strains $e_{33}$ and $e_{11}$, respectively. Equivalently, $\gamma_{33}, \gamma_{13}$ give the stresses $\sigma_{33}, \sigma_{11}$ induced on the unit cell by an electric field along the *c* axis. The former relationship underlies the earlier work of Dal Corso *et al.*[9] based on finite-difference formulas and geometric phase, and the latter is used in the present work based on DFT linear response.

To obtain the piezoelectric and dielectric constants, we perform two DFT-LR calculations, one with phonon perturbations corresponding to Zn and O displacements along the *c* axis, and another with a perturbing electric field along the *c* axis. The phonon perturbation allows us to obtain both the frequencies of the $\Gamma$-point phonons with *z* polarization (which are proportional to the square roots of the respective force constants, $\sqrt{K_\alpha}$), and the strain-phonon couplings, $L_{\alpha,zz}$ and $L_{\alpha,xx}$. The LR calculations with the electric-field perturbation yield the optical dielectric constant $\epsilon_{33}^{\infty}$, the Born effective charges $Z_{\alpha,zz}$, and the clamped-ion piezoelectric couplings $\gamma_{33}^0$ and $\gamma_{13}^0$. The dielectric and piezoelectric constants are then given by

$$\epsilon_{33} = \epsilon_{33}^{\infty} + 4\pi \sum_{\alpha} \frac{Z_{\alpha,zz} Z_{\alpha,zz}}{K_\alpha},$$

$$\gamma_{33} = \gamma_{33}^0 + \sum_{\alpha} \frac{Z_{\alpha,zz} L_{\alpha,zz}}{K_\alpha},$$

$$\gamma_{13} = \gamma_{13}^0 + \sum_{\alpha} \frac{Z_{\alpha,zz} L_{\alpha,xx}}{K_\alpha}.$$

### C. Technical details

All calculations were performed on Silicon Graphics O2 and Origin 200 systems using the conjugate gradient program CASTEP 2.1 (Refs. 26 and 27) and our own related density functional linear response program.[28] We used a plane-wave cutoff of 64 Ry, which corresponds to around 3000 plane waves per wave function in a single ZnO wurtzite unit cell. A $3\times3\times2$ Monkhorst-Pack[29] grid was used, leading to six *k* points in the irreducible Brillouin zone for the high symmetry structures, and a correspondingly higher number for distorted structures with lower symmetry. The exchange correlation was parametrized using the Perdew-Zunger parametrization[30] of the Ceperley-Alder potential.[31]

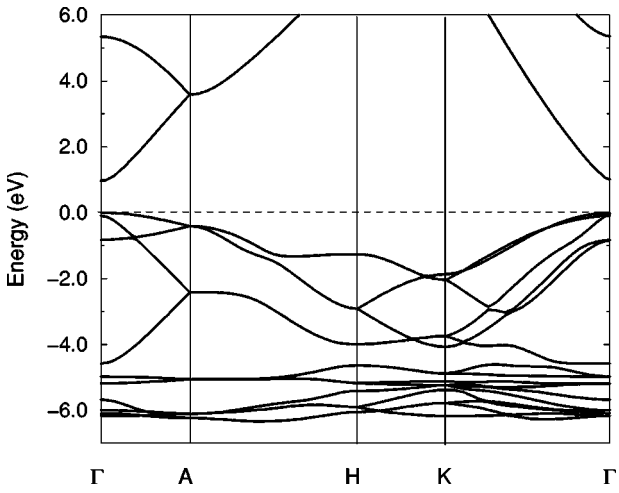


FIG. 2. Calculated band structure of ZnO.

## IV. UNSTRAINED ZNO; NEW RESULTS AND COMPARISON WITH LAPW CALCULATIONS

Before presenting our results for strained ZnO, we first discuss bulk, unstrained ZnO, and compare the results of our plane-wave pseudopotential calculations with published theoretical and experimental data. A good test of the transferability of the pseudopotentials is that they predict the same minimum energy structure as all-electron calculations which use the same approximation for the exchange-correlation functional. The minimum energy volume obtained by the earlier all-electron LDA calculation (Ref. 9) is 45.89 Å$^3$. Reference 9 also showed that the LDA $c/a$ ratio and $u$ value are the same as the corresponding experimental quantities to within 0.5 mRy, and that the energy surface is rather flat around the minimum in the $(u, c/a)$ plane. The minimum energy volume obtained using our pseudopotentials is 47.6 Å$^3$ (at the experimental $c/a$ ratio and $u$ value), and that obtained by an earlier pseudopotential calculation using a Gaussian basis is 46.80 Å$^3$. The experimental volume is 47.90 Å$^3$ and we believe the results obtained using our method are within LDA errors.

### A. Band-structure analysis

In Fig. 2 we show the calculated band structure for ZnO at the experimental unit-cell volume ($a=3.2595$ Å, $c=5.2070$ Å, and $u=0.3820$), which is approximately equal to the LDA minimum volume for our pseudopotentials. The top of the valence band is set to 0 eV. The band structure is indistinguishable from that presented in Ref. 9, which was calculated using the FLAPW technique.

The narrow bands between around $-6$ and $-5$ eV derive largely from the Zn $3d$ orbitals and are completely filled. The broad bands between around $-5$ and 0 eV are from the O $2p$ orbitals and are again completely filled. The Zn $4s$ band is broad and unoccupied, ranging between 1 and 7 eV above the band gap. Figure 3 shows the same band structure along $\Gamma$ to A with the symmetry labels within the $C_{6v}$ group added. 1 is the totally symmetric representation, 2

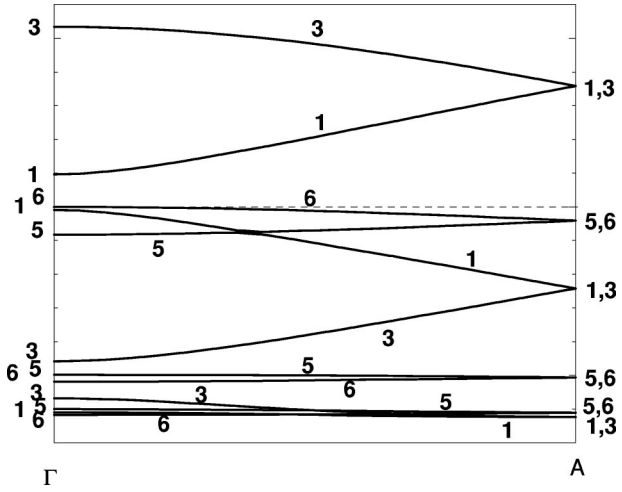


FIG. 3. Band structure of ZnO along the Γ to A symmetry line with symmetry labels added. The energy range is from −7 to 6 eV with the tick marks in 1 eV spacing, and the Fermi energy (0 eV) is shown by the dashed line.

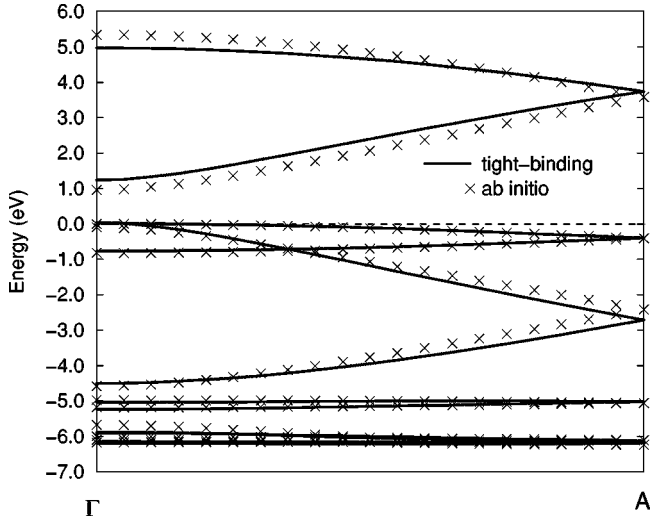


FIG. 4. Comparison of tight-binding and *ab initio* band structures in ZnO.

is antisymmetric with respect to $C_6$ and $C_2$ rotation and $\sigma_v$ reflection, 5 and 6 are the doubly degenerate representations, with 5 being antisymmetric with respect to $C_6$ and $C_3$ rotation, and 6 being antisymmetric with respect to $C_3$ and $C_2$ rotation. We see that interactions between O $2p$ and Zn $3d$ orbitals are allowed by symmetry at Γ and A, and along the adjoining Δ line. The Zn $s$ orbitals can interact with O $2p$ and Zn $3d$ bands of 1 and 3 symmetry.

In order to quantify the interactions between the various orbitals we perform a tight-binding analysis along the Γ to A direction of the Brillouin zone. Tight-binding parameters are obtained by nonlinear-least-squares fitting[32] to the calculated *ab initio* energies at the high symmetry Γ and A points, and at 19 points along the Δ axis. A good tight-binding fit (rms deviation=0.11) is obtained when only nearest-neighbor interactions between O $2p$ and Zn $3d$ bands, and O $2p$ and Zn $4s$ bands are included in the fit. Additional small Zn $3d$–Zn $3d$ interactions are needed to produce dispersion in the upper $e_g$ Zn $3d$ band along this symmetry axis. The tight-binding parameters which we obtain are given in Table II (in the column labeled ''structure 1''), and the tight-binding band structure is compared with the *ab initio* band structure in Fig. 4.

The two sets of Zn-O parameters correspond to the two Zn-O distances, the shorter ($r_1=1.974$ Å) being the separation of the Zn and O atoms lying directly above each other along the $c$ direction, and the longer ($r_2=1.989$ Å) joining Zn and O atoms in adjacent $c$-oriented ''chains.'' The Zn $3d$–Zn $3d$ interactions are small. The Zn $4s$–O $2p$ interactions are large, and show the expected increase when the Zn-O spacing is decreased. The Zn $3d$–O $2p$ interactions are also large, and are quite different (even changing sign) for the two different Zn-O atom pair types. In fact both the $\sigma$ and $\pi$ components are *larger* for the in-plane pairs which have the larger Zn-O spacing. This distance dependence is unusual for tight-binding parameters, and suggests that the nature of the Zn $3d$–O $2p$ hybridization is different for the Zn-O pairs lying in the $c$ axis chains, than for the basal plane Zn-O pairs.

### B. Piezoelectric and dielectric properties

In Table I, we present our results for piezoelectric and dielectric compliances and a comparison with those obtained in previous FLAPW calculations[9] and experiments.[33] The agreement between the computational results is good, but the scatter in experimental results indicates that the piezoelectric constants may be sensitive to experimental conditions. We will investigate this issue in the next section. We also report in Table I the frequencies of TO phonons with $c$ polarization at the Γ point, and note that only one of the TO phonons

TABLE I. Comparison between results of FLAPW calculations (Ref. 9), pseudopotential calculations (this work) and experimental results (Ref. 33) for piezoelectric constants and related properties of ZnO.

| Property | Ref. 9 | Present work | Experiment (Ref. 33) |
|---|---|---|---|
| $Z^{\star}_{\mathrm{Zn},z}$ | 2.05 | 2.07 | 2.10 |
| $\gamma^0_{33}$ (C/m$^2$) | −0.58 | −0.73 | |
| $\gamma_{33}$ (C/m$^2$) | 1.21 | 1.30 | 1.0-1.5 |
| $\gamma^0_{13}$ (C/m$^2$) | 0.37 | 0.31 | |
| $\gamma_{13}$ (C/m$^2$) | −0.51 | −0.66 | −0.36 to −0.62 |
| $\epsilon^{\infty}_{33}$ | | 4.39 | |
| $\epsilon_{33}$ | | 8.75 | |
| TO phonon (cm$^{-1}$) | | 544.919, 395.349, 258.519 | |

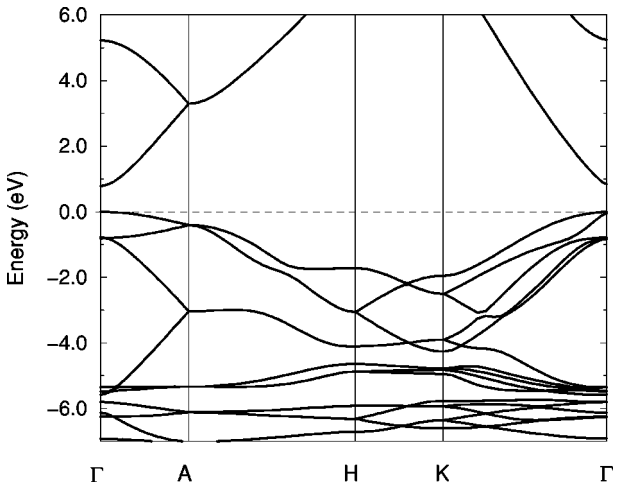


FIG. 5. Calculated band structure of strained ZnO.

(395 $cm^{-1}$) is IR active; this is the only phonon which contributes to piezoelectric and dielectric constants $\gamma_{33}$, $\gamma_{13}$, and $\epsilon_{33}$, studied in this work. Our results also confirm the conclusion of Ref. 9 that the piezoelectric constants of ZnO are dominantly contributed by phonons (internal strain). The dielectric constant, on the other hand, has roughly equal contributions from electrons ($\epsilon^{\infty}$) and phonons.

## V. EFFECTS OF STRAIN AND TEMPERATURE ON THE ELECTRONIC PROPERTIES OF BULK ZnO

### A. Band structures

Next we investigate the effects of strain on the static electronic properties of bulk ZnO. We compare two different strained structures with the equilibrium structure at the experimental lattice constant. First, we simulate application of a homogeneous in-plane compression by reducing the *a* lattice constant by 2%, while increasing the *c* lattice constant correspondingly to maintain the same total volume. The value of *u* is held at 0.3820 of the *c* axis. Second, we investigate the effect of changing the Zn-O separation along the *c* axis, *u*, by increasing it by 5% to 0.4011, while retaining the equilibrium *a* and *c* values.

#### *1. In-plane compression*

Application of the in-plane compression to reduce the *a* lattice constant by 2% increases the total energy by 0.1 eV, and creates Hellman-Feynman forces on the atoms in the *z* direction of $\pm 0.59$ eV/Å. The band structure of the compressed structure is shown in Fig. 5. We observe a broadening of the bands, as expected from the increased overlap between the orbitals in the basal plane. Note in particular the broadening in the Zn $3d$ bands. In spite of the fact that the *d* bands are narrow, they are very sensitive to strain and bond length as a result of $p$-$d$ hybridization processes.

In addition to an overall band broadening, there are a number of significant details in the band structure for this compressed structure. First, the O $2p$ bands with symmetries 1 and 3 shift down relative to the uppermost O $2p$ bands at the Γ point. This leads to a reduction in the density of states at the Fermi level, and to an overlapping of the low-energy part of these bands with the Zn $3d$ bands. The ordering of the lower Zn $3d$ bands is reversed compared with those in the unstrained structure, and the Zn $4s$ bands shift slightly down in energy, resulting in a smaller band gap.

These observations are consistent with a tight-binding fit along the Γ to *A* line, the results of which are given in Table II (structure 2). Again, a good (root-mean-square deviation $=0.11$) tight-binding fit is obtained using the limited interaction set described above. Again the O $2p$–Zn $4s$ hybridization is large and shows the expected variation with bond length. The dependence of the (also large) $p$-$d$ parameters on distance does not follow a straightforward pattern. Note that the anomalously low value for the Zn $4s$ energy is the result of an attempt by the fitting package to reproduce the down shift in the O $2p$ band of 1 symmetry (which also contains a significant Zn $4s$ component) within our limited basis set. This energy value shifts up to a more physical positive number if additional interactions are included in the basis.

TABLE II. Tight-binding parameters (in eV) for ZnO obtained by non-linear-least-squares fitting to the *ab initio* eigenvalues along Γ to *A*. *E* indicates an orbital energy, and *V* an interatomic transfer integral. The transfer integrals with the superscript ''1'' are between the closest nearest-neighbor Zn-O pairs, and those with the superscript ''2'' are between the nearest neighbors with the larger separation. Only the parameters listed in the table were allowed to be nonzero in the fitting procedure.

| Parameter | Structure 1 | Structure 2 | Structure 3 |
|---|---|---|---|
| $E_{\mathrm{O}\ 2p}$ | −1.262 | −1.062 | −1.308 |
| $E_{\mathrm{Zn}\ 4s}$ | 1.235 | −0.274 | 1.409 |
| $E_{\mathrm{Zn}\ 3d}$ | −5.144 | −5.396 | −5.159 |
| $V^1_{\mathrm{O}\ 2p\text{–}\mathrm{Zn}\ 4s}$ | 2.584 | 2.936 | 2.823 |
| $V^2_{\mathrm{O}\ 2p\text{–}\mathrm{Zn}\ 4s}$ | 2.386 | 2.517 | 2.279 |
| $V^1_{(\mathrm{O}\ 2p\text{–}\mathrm{Zn}\ 3d)\sigma}$ | 0.625 | 0.829 | 0.591 |
| $V^2_{(\mathrm{O}\ 2p\text{–}\mathrm{Zn}\ 3d)\sigma}$ | −0.856 | −1.343 | −0.761 |
| $V^1_{(\mathrm{O}\ 2p\text{–}\mathrm{Zn}\ 3d)\pi}$ | 1.292 | 1.444 | 1.294 |
| $V^2_{(\mathrm{O}\ 2p\text{–}\mathrm{Zn}\ 3d)\pi}$ | −1.711 | −1.365 | −1.802 |
| $V_{(\mathrm{Zn}\ 3d\text{–}\mathrm{Zn}\ 3d)\sigma}$ | 0.169 | 0.124 | 0.170 |
| $V_{(\mathrm{Zn}\ 3d\text{–}\mathrm{Zn}\ 3d)\pi}$ | −0.006 | 0.001 | −0.014 |
| $V_{(\mathrm{Zn}\ 3d\text{–}\mathrm{Zn}\ 3d)\delta}$ | 0.053 | 0.034 | 0.060 |

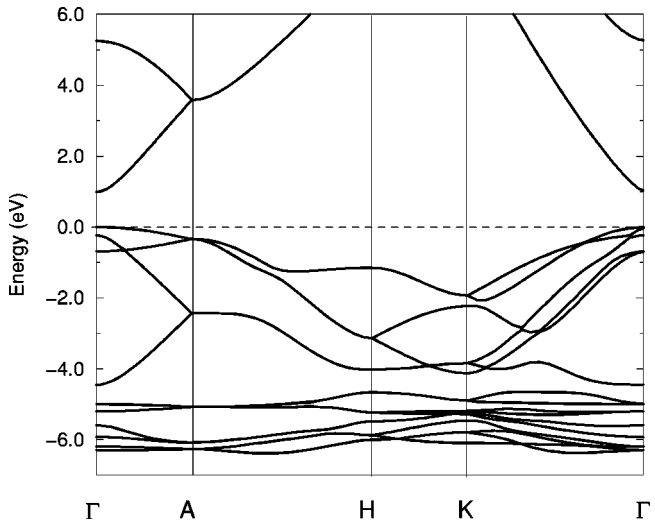


FIG. 6. Calculated band structure of ZnO with the $u$ value increased by 5%.

#### 2. Change in u value

Change in the $u$ value by 5% increases the total energy by only 0.07 eV compared with the equilibrium structure, and introduces Hellman-Feynman forces of $\pm 0.59$ eV in the $z$ direction on the ions. The new band structure is shown in Fig. 6, and is qualitatively very similar to that of the undistorted structure.

A tight-binding fit using the interaction set described above produces an rms deviation of 0.13, and the parameters listed in Table II. Again the O $2p$–Zn $4s$ interaction is largest for the smallest bond length as expected, but the $p$-$d$ hybridizations have a more complicated distance dependence. In this case, the O $2p$ bands with 1 and 3 symmetries are shifted down a small amount at $\Gamma$, but not as much as in the previous structure. As a result they do not overlap with the Zn $3d$ bands. The Zn $4s$ bands are not shifted down relative to their position in the unstrained case.

### B. Piezoelectric properties

#### 1. Stress dependence

Finally, we explore the piezoelectric and dielectric properties of strained ZnO in detail. As a result of anharmonic couplings between different phonons and strain, the properties of ZnO are strongly structure sensitive. There is a large region in the phase space of structural configurations which is low in energy and therefore contributes to the properties of ZnO. To obtain energies, polarization and other properties for each of these configurations from first principles is inefficient and impractical. We choose instead to use a model energy functional that captures the physics of the low-energy structural excitations of ZnO.

To keep the model simple, we restrict our analysis to the subspace of degrees of freedom that preserve the symmetry of the wurtzite structure $\{x=e_{xx}=e_{yy}, z=e_{zz}, u\}$. Justification for this simplification rests on the assumption (verifiable through *ab initio* calculations) that most of the low-energy configurations preserve wurtzite symmetry and most of the symmetry-breaking distortions are described well at harmonic order and can be integrated out. This is in contrast with earlier work on structural phase transitions[18] where the symmetry-breaking distortions were retained in the subspace.

We write the model energy functional as a symmetry-invariant Taylor expansion in atomic displacements (or normal mode degrees of freedom $u$) and strains $(x,z)$ defined above. Including the lowest order coupling with external stress $\sigma_\alpha$ and electric field along the $c$ axis $E$,

$$E_{tot}(x,z,u,\sigma_\alpha,E)=\frac{1}{2}Ku^2+Au^3+Bu^4+\frac{1}{2}[C_x x^2+C_z z^2+C_{xz}xz]+D_x x^3+E_x x^4+D_z z^3+E_z z^4+\sum_\alpha F_\alpha r_\alpha u^2$$
$$+\sum_{\alpha,\beta} G_{\alpha\beta} r_\alpha r_\beta u+\sum_{\alpha,\beta} H_{\alpha\beta} r_\alpha r_\beta u^2-\Omega(2\sigma_x x+\sigma_z z+2\gamma^0_{13}xE+\gamma^0_{33}zE)-ZuE-\frac{\Omega}{4\pi}\epsilon_\infty E^2, \quad (1)$$

where the $\gamma^0$'s and $\epsilon_\infty$ are clamped (or electronic) piezoelectric and dielectric constants, and $r_\alpha$ is strain $x$ or $z$. $K$, $A \ldots H$, $\gamma$, and $\epsilon$ are the harmonic and anharmonic coupling parameters including force, elastic, and mixed coupling constants. These parameters have been determined from DFT total energy and linear-response calculations.

The equilibrium state of ZnO under the application of external stress or electric field at zero kelvin is obtained by minimizing the total energy $E_{tot}$ with respect to the structural parameters $x$, $z$, and $u$:

$$\frac{\partial E_{tot}}{\partial x}=0, \quad \frac{\partial E_{tot}}{\partial z}=0, \quad \frac{\partial E_{tot}}{\partial u}=0. \quad (2)$$

For the equilibrium structure, the static dielectric and piezoelectric constants are calculated using the expressions in Sec. III (also in Ref. 23), with various coupling parameters being dependent on the structure. The spontaneous polarization is calculated using the expression

$$P=-\frac{\partial E_{tot}}{\partial E}.$$

ZnO is grown in the form of thin solid films on sapphire and there are always interfacial stresses in the films. We use our model to study properties of ZnO as a function of stress in the basal $ab$ plane. In Fig. 7, we show our results for the structural parameter $u$, dielectric and piezoelectric response of ZnO as the applied stress $\sigma=\sigma_{xx}=\sigma_{yy}$ is varied from $-1$ to 1 GPa.

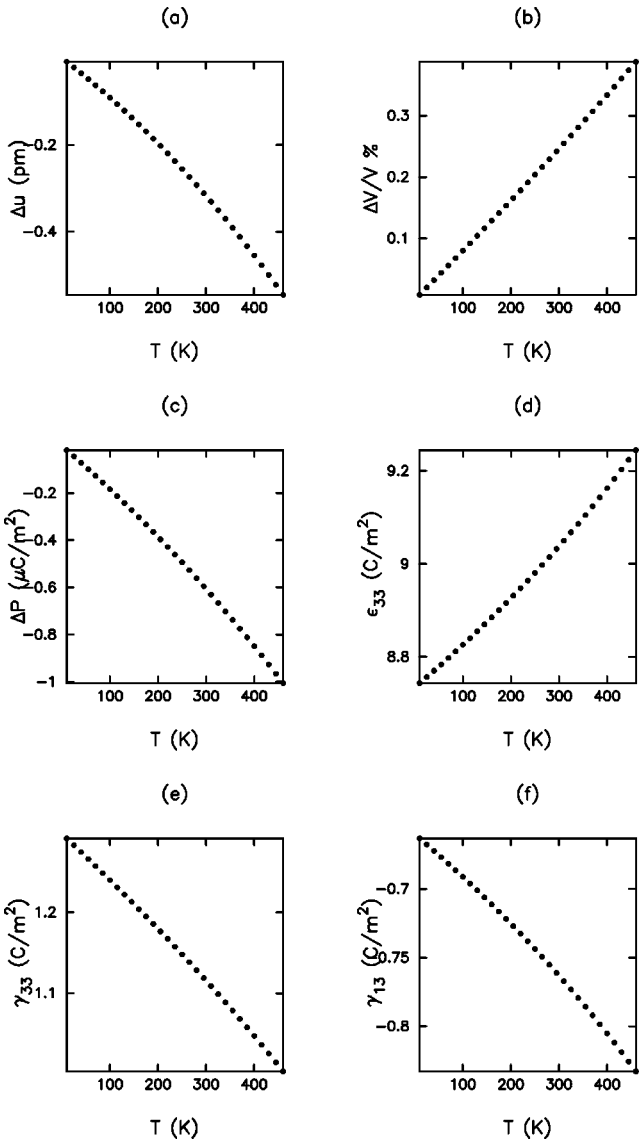


FIG. 7. Dependence of the change in structural parameter $\Delta u$ (a), dielectric $\epsilon_{33}$ (b), piezoelectric constants $\gamma_{33}$ (c) and $\gamma_{13}$ (c) of ZnO on the applied stress in the basal plane $\sigma=\sigma_{xx}=\sigma_{yy}$.

We find that parameter $u$ changes by about 1% in this range of basal stress. The dielectric constant $\epsilon_{33}$ monotonically increases by about 2–3 %. In contrast, the piezoelectric constants are rather sensitive to stress changing by about 15–30 %. With access to different contributions to these constants in our model, we discover that most of the dependence of these compliances on stress is due to the phonon contribution.

### *2. Temperature dependence*

ZnO is also a pyroelectric material, characterized by a temperature dependence of the polarization. This has technological relevance because it leads to the widespread use of ZnO in infrared detectors. To explore various stress and electric-field-dependent properties of ZnO at finite temperature, we obtain a free-energy functional using a local harmonic model[34] for entropy. In this model, entropy is calculated treating phonons harmonically for given structural parameters. In the present work, we include the optical phonons that are polarized along the $z$ axis. With these approximations, the free energy is

$$G(x,z,u,\sigma_x,\sigma_z,E,T)=E_{tot}(x,z,u,\sigma_x,\sigma_z,E)+3k_BT\ln\left(\frac{(K_1K_2K_3)^{1/3}}{k_BT}\right), \quad (3)$$

where the $K_i$'s are the harmonic force constants of the three $\Gamma$ phonons with $z$ polarization for given values of structural parameters. Due to the anharmonic terms included in the energy expansion Eq. (1), $K_i$'s (hence the $T$-dependent part of the free energy) depend on the structure. The equilibrium state of ZnO under the application of external stress or electric field at finite temperature is then obtained by minimizing the free energy $G$ with respect to the structural parameters $x$, $z$, and $u$:

$$\frac{\partial G}{\partial x}=0, \quad \frac{\partial G}{\partial z}=0, \quad \frac{\partial G}{\partial u}=0. \quad (4)$$

Again, the dielectric and piezoelectric constants are calculated using the expressions in Sec. III, and the spontaneous polarization is now calculated using the expression

$$P=-\frac{\partial G}{\partial E}.$$

We investigate the dependence of various properties of ZnO on temperature. In Fig. 8, we display results for structural parameters, dielectric and piezoelectric constants, and polarization for a range of temperatures from 0 to 450 K. We find that the structural parameters such as the bond-length $u$ and volume change only by about 0.3% from 0 K to room temperature.

The pyroelectric constant, which we obtain from our calculated results for polarization, is 20 $\mu$C/m$^2$/K, compared with the experimental value of 9.4 $\mu$C/m$^2$/K.[33] Considering the simplicity in our treatment of temperature through the model entropy function, we find this agreement quite encouraging. In particular, we point out that, while the nonpolar TO phonons with $z$ polarization have been omitted from the expansion of energy, they *have* been included in the entropy term, where we use the expression of entropy[34] treating phonons harmonically, consistent with our energy expansion.

To estimate the effect of these nonpolar phonons on the pyroelectric constant, we omitted their contribution to entropy and found a pyroelectric constant of about 40 $\mu$C/m$^2$/K (almost doubled). If we assume that phonons should generally suppress the pyroelectric constant, the discrepancy between theory and experiment is likely due to our omission of phonons with $x$ and $y$ polarization from the entropy expression.

The linear dielectric response $\epsilon_{33}$ of ZnO is quite sensitive to temperature, changing by about 4% in the temperature range considered. The piezoelectric response, on the other hand, is very sensitive to temperature changing by about 20%. This should be an important consideration in designing piezoelectric devices for operation at room temperature.

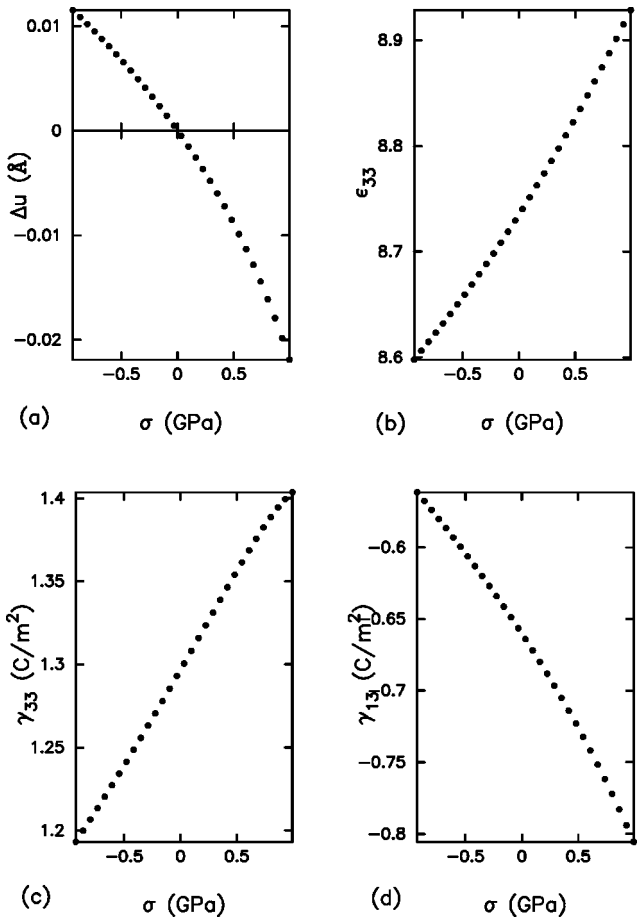


FIG. 8. Dependence of the change in structural parameter $\Delta u$ (a), volume $\Delta V/V$ (b), and spontaneous polarization $\Delta P$ (c), dielectric constant $\epsilon_{33}$ (d), piezoelectric constants $\gamma_{33}$ (e), and $\gamma_{13}$ (f) of ZnO on the temperature.

### C. Discussion

It is clear from our results that the piezoelectric response of ZnO is strongly sensitive to both temperature and stress, changing by up to 30% over the range of parameters considered. This dependence arises from the changes in structural parameters (manifested through the phonon contribution). We saw in Sec. III that the phonon contribution to the piezoelectric constants arises from the coupling of phonons with strain, $L$, and Born effective charge, $Z$,

$$\gamma_{phonon}=\frac{L\cdot Z}{K},$$

$K$ being the force constant. In Fig. 9, we show how $K$ and $L$ for the polar TO phonon change with temperature. While $K$ changes by only 10%, the coupling with strain $L$ changes by about 25%. The Born effective charge $Z$ (which describes the coupling of this phonon with electric field) is not found to vary much with temperature. The large temperature dependence of the piezoelectric response arises predominantly from that of the coupling of phonon with strain and its force constant. Since only the latter contributes to the dielectric constants, dielectric properties are less sensitive to structure, stress, or temperature.

In Sec. V A, we found the hybridization between Zn $d$ orbitals and O $p$ orbitals to be sensitive to structural parameters. The same hybridization was found to be the cause of anomalous Born effective charges in ferroelectric materials such as $PbTiO_3$.[3] While the $d$ orbitals of the transition metals in perovskite ferroelectrics are formally unoccupied, those in Zn are fully occupied, leading to normal effective charges. The coupling of phonons with strain, however, is large and structure dependent irrespective of the occupancy of $d$ orbitals.

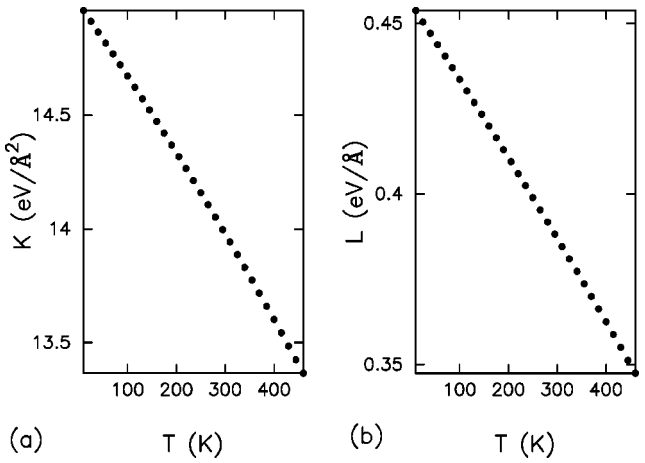


FIG. 9. Dependence of (a) the force constant and (b) coupling with the strain of the polar TO phonon as a function of temperature.

## VI. SUMMARY

In summary, we have calculated the electronic and atomic structure of ZnO from first principles, and analyzed the nature of the bonding using the tight-binding method. We find that hybridization between the Zn $d$ orbitals and O $p$ orbitals is strongly structure dependent. Using DFT linear response, we have obtained the phonon frequencies, dielectric and piezoelectric constants of ZnO at zero temperature, and have shown that phonons (internal strain) have the dominant contribution to piezoelectricity in ZnO. From DFT linear-response and total-energy calculations, and a simple model for vibrational entropy, we have constructed an *ab initio* free-energy functional for ZnO to study its properties at finite temperature and under applied stress. Our results show that the piezoelectric properties of ZnO are strongly dependent on both temperature and stress. This clearly has implications for the design of devices intended to operate at room temperature, or under stressed conditions. By analyzing various physical contributions, we have found that this is primarily due to the coupling between phonons and strain. The O $2p$–Zn $3d$ hybridization is the cause of the large magnitude and sensitivity of this coupling.

## ACKNOWLEDGMENTS

The authors thank Andrew Rappe and Nicholas Ramer for their assistance in generating the Zn pseudopotential, and Paul Verghese and V. Srikant for many useful discussions. Many of the ideas presented in this paper were formulated during the 1998 ''Physics of Insulators'' workshop at the Aspen Center for Physics. N.A.H.'s funding was provided through the NSF-POWRE program, Grant No. DMR-9973859. U.V.W.'s funding was provided by the Office of Naval Research, Grant No. N00014-97-1-1068.

*Present address: Theoretical Sciences Unit, J. Nehru Center for Advanced Scientific Research, Jakkur, Bangalore, 560 064, India.

[1] A. Ahmin, J. Am. Ceram. Soc. **72**, 369 (1989).
[2] R. E. Cohen and H. Krakauer, Ferroelectrics **136**, 95 (1992).
[3] R. E. Cohen, Nature (London) **358**, 136 (1992).
[4] J. C. Phillips and L. Kleinman, Phys. Rev. **116**, 287 (1959).
[5] U. Rossler, Phys. Rev. **184**, 733 (1969).
[6] S. Bloom and I. Ortenburger, Phys. Status Solidi B **58**, 561 (1973).
[7] J. R. Chelikowsky, Solid State Commun. **22**, 351 (1977).
[8] P. Schröer, P. Krüger, and J. Pollmann, Phys. Rev. B **47**, 6971 (1993).
[9] A. Dal Corso, M. Posternak, R. Resta, and A. Baldereschi, Phys. Rev. B **50**, 10 715 (1994).
[10] J. E. Jaffe and A. C. Hess, Phys. Rev. B **48**, 7903 (1993).
[11] J. E. Jaffe, N. M. Harrison, and A. C. Hess, Phys. Rev. B **49**, 11 153 (1994).
[12] M. T. Yin and M. L. Cohen, Phys. Rev. B **26**, 5668 (1982).
[13] H. Hohenberg and W. Kohn, Phys. Rev. **136**, B864 (1964); W. Kohn and L. J. Sham, *ibid.* **140**, B1133 (1965).
[14] P. Bendt and A. Zunger, Phys. Rev. Lett. **50**, 1684 (1983).
[15] X. Gonze, Phys. Rev. B **55**, 10 337 (1997).
[16] J. L. Martins, N. Troullier, and S.-H. Wei, Phys. Rev. B **43**, 2213 (1991).
[17] A. M. Rappe, K. M. Rabe, E. Kaxiras, and J. D. Joannopolous, Phys. Rev. B **41**, 1227 (1990).
[18] U. V. Waghmare and K. M. Rabe, Phys. Rev. B **55**, 6161 (1997).
[19] N. A. Hill and K. M. Rabe, Phys. Rev. B **59**, 8759 (1999).
[20] S. G. Louie, S. Froyen, and M. L. Cohen, Phys. Rev. B **26**, 1738 (1982).
[21] L. Kleinman and D. M. Bylander, Phys. Rev. Lett. **48**, 1425 (1982).
[22] X. Gonze, P. Käckell, and M. Scheffler, Phys. Rev. B **41**, 12 264 (1990).
[23] U. V. Waghmare (unpublished).
[24] X. Gonze, D. C. Allan, and M. P. Teter, Phys. Rev. Lett. **68**, 3603 (1992).
[25] O. H. Nielsen and R. M. Martin, Phys. Rev. B **32**, 3792 (1985).
[26] M. C. Payne, M. P. Teter, D. C. Allan, T. A. Arias, and J. D. Joannopoulos, Rev. Mod. Phys. **64**, 1045 (1992).
[27] M. C. Payne, X. Weng, B. Hammer, G. Francis, U. Bertram, A. de Vita, J. S. Lin, V. Milman, and A. Qteish (unpublished).
[28] U. V. Waghmare, K. M. Rabe, and V. Milman (unpublished).
[29] H. J. Monkhorst and J. D. Pack, Phys. Rev. B **13**, 5188 (1976).
[30] J. P. Perdew and A. Zunger, Phys. Rev. B **23**, 5048 (1981).
[31] D. M. Ceperley and B. J. Alder, Phys. Rev. Lett. **45**, 566 (1980).
[32] L. F. Mattheiss, Phys. Rev. B **6**, 4718 (1972).
[33] *Elastic, Piezoelectric, Pyroelectric, Piezooptic, Electrooptik Constants, and Nonlinear Dielectric Susceptibilities of Crystals*, edited by K. H. Hellwege and A. M. Hellwege, Landolt-Börnstein, New Series, Group III, Vol. 11 (Springer, Berlin, 1979).
[34] R. LeSar, R. Najafabadi, and D. J. Srolovitz, Phys. Rev. Lett. **63**, 624 (1989).